VIP Microporous Materials Very Important Paper

International Edition: DOI: 10.1002/anie.201807506
German Edition: DOI: 10.1002/ange.201807506

Carving Out Pores in Redox-Active One-Dimensional Coordination Polymers

Naomi E. Clayman[+], Mary Anne Manumpil[+], Daiki Umeyama, Andrey E. Rudenko, Hemamala I. Karunadasa, and Robert M. Waymouth**

Abstract: *Reduction of the insulating one-dimensional coordination polymer $[Cu(abpy)PF_6]_n$, **1a**(PF_6), (abpy = 2,2′-azobispyridine) yields the conductive, porous polymer $[Cu(abpy)]_n$, **2a**. Pressed pellets of neutral **2a** exhibit a conductivity of 0.093 S cm^{-1} at room temperature and a Brunauer–Emmett–Teller (BET) surface area of 56 m^2 g^{-1}. Fine powders of **2a** have a BET surface area of 90 m^2 g^{-1}. Cyclic voltammetry shows that the reduction of **1a**(PF_6) to **2a** is quasi-reversible, indicative of facile charge transfer through the bulk material. The BET surface area of the reduced polymer **2** can be controlled by changing the size of the counteranion X in the cationic $[Cu(abpy)X]_n$. Reduction of $[Cu(abpy)X]_n$ with X = Br (**2b**) or BAr^F (**2c**; BAr^F = tetrakis(3,5-bis(trifluoromethyl)-phenyl)), affords $[Cu(abpy)]_n$ polymers with surface areas of 60 and 200 m^2 g^{-1}, respectively.*

Coordination polymers[1] and other classes of metal-containing macromolecules combine the electronic properties of inorganic complexes with macromolecular behavior. Owing to their unique combination of properties, metallopolymers[2–9] have elicited significant interest as materials for sensors,[3–5] microelectronics,[6,10,11] energy storage,[7,8] gas separation,[9] and catalysis.[9,12] Although there are many examples of redox-active and electrically conductive metallopolymers,[6,13–17] few are porous.[12] Whereas porosity in network solids, such as three-dimensional metal–organic frameworks, arises from voids in the framework,[1,9,18] porosity in 1D coordination polymers depends on how the polymer chains pack in the solid state. Herein, we report a method to generate porous conductive coordination polymers by reduction of cationic polymers; extrusion of counterions provides a means of generating and tuning the porosity.

Electrochemical or chemical reduction with cobaltocene (Cp_2Co) of an acetonitrile (MeCN) solution of the blue, insulating, cationic coordination polymer $[Cu(abpy)PF_6]_n$, **1a**(PF_6),[19] results in the precipitation of a black insoluble material (Figure 1). Inductively coupled plasma atomic emission spectroscopy (ICP-AES) and combustion analysis of the polymer support assignment of the approximate formula $[Cu(abpy)]_n$ for **2a**, with trace contamination from residual Co and PF_6 (Supporting Information). Analysis of **2a** by matrix-assisted laser desorption ionization time-of-flight (MALDI-TOF) mass spectrometry reveals ions corresponding to short chains of the copper–azobispyridine repeat unit $Cu_n(abpy)_x$ (Supporting Information, Figure S1).

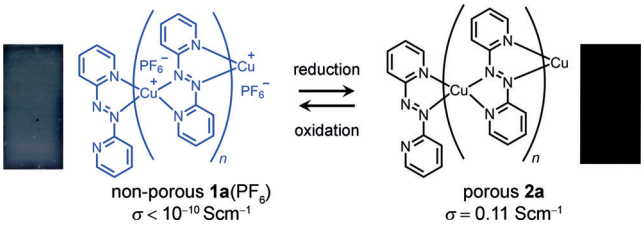

Figure 1. Non-porous and insulating $[Cu(abpy)PF_6]_n$, **1a**(PF_6), reversibly transforms to porous and conductive $[Cu(abpy)]_n$, **2a**, upon reduction. Films of **1a**(PF_6) and **2a** are blue (left) and black (right), respectively.

The reduction of **1a**(PF_6) to **2a** results in both an increase in porosity and a significant increase in conductivity. The cationic coordination polymer **1a**(PF_6) exhibits negligible porosity, whereas powders of the reduced neutral polymer **2a** exhibit a Brunauer–Emmett–Teller (BET) surface area of 90 m^2 g^{-1}. Four-point-probe conductivity measurements on pressed pellets of **2a** yielded conductivities approaching 0.11 S cm^{-1} at room temperature (Table 1). In contrast, pressed pellets of the cationic metallopolymer **1a**(PF_6) exhibits an upper limit of conductivity of about 10^{-10} S cm^{-1} (corresponding to instrumental detection limits; Supporting Information, Figure S2).

Addition of an acetonitrile solution of ferrocenium hexafluorophosphate (Cp_2FePF_6) to the insoluble reduced

Table 1: Surface area and conductivity values for **2**.[a]

$[Cu(abpy)]_n$	Departed anion	BET surface area [m^2 g^{-1}]		Conductivity ($\times 10^{-2}$ S cm^{-1}) pressed pellet, 25 °C	
		powder	pellet[a]	*a*	*b*
2a	PF_6^-	90	56	9.3	11
2b	Br^-	60	52	1.7	3.5
2c	BAr^{F-}	200	110	3.1	3.5

[a] Pellets pressed at *a*) 14.5 kN for 1.5 h and *b*) 22 kN, 12 h.

[*] N. E. Clayman,[+] M. A. Manumpil,[+] D. Umeyama, A. E. Rudenko, H. I. Karunadasa, R. M. Waymouth
Department of Chemistry, Stanford University
Stanford, CA 94305 (USA)
E-mail: hemamala@stanford.edu
waymouth@stanford.edu

D. Umeyama
Present Address: International Center for Materials Nanoarchitectonics (MANA), National Institute for Materials Science (NIMS)
1-1 Namiki, Tsukuba, Ibaraki 305-0044 (Japan)

[+] These authors contributed equally to this work.

Supporting information and the ORCID identification number(s) for the author(s) of this article can be found under: https://doi.org/10.1002/anie.201807506.

polymer **2a** results in the re-dissolution of all material and re-speciation of all copper species as **1a**(PF_6). The reversible deposition and dissolution can also be performed electrochemically: electrochemical reduction of **1a**(PF_6) by controlled-potential electrolysis at −0.7 V vs. $Ag/AgNO_3$ results in the deposition of a black film of **2a** on the working electrode (Supporting Information, Figure S4). When the polarity of the electrochemical cell is reversed, all material deposited on the electrode is dissolved to regenerate the cationic polymer **1**(PF_6).

Owing to the insolubility of the reduced polymer **2a**, attempts to grow crystals suitable for single-crystal X-ray diffraction were unsuccessful. However, microcrystalline sheets of **2a** could be deposited directly on indium tin oxide (ITO) electrodes in an electrochemical cell containing **1**(PF_6) by oscillating the potential around the $E_{1/2}$ of the **1a**(PF_6)/**2a** redox couple. The synchrotron powder X-ray diffraction pattern of **2a** displays some long-range order (Supporting Information, Figure S5). Scanning electron microscopy (SEM) reveals that **2a** forms as slip-stacked sheets on ITO (Supporting Information, Figure S6). To provide further information on the structure of **2a**, we performed X-ray scattering experiments (beamline 11-ID-B, Advanced Photon Source, Argonne National Laboratory) and analyzed the pair distribution function (PDF) of the total X-ray scattering data. The PDF of the $[Cu(abpy)BF_4]_n$ coordination polymer (**1**BF_4)[19] with the BF_4^- anions removed was simulated from the reported crystal structure. This simulated PDF matched well with the experimental PDF of **2a** (Figure 2A), including the covalent bond lengths in abpy (C–N and C–C ca. 1.4 Å), coordination bond length (N–Cu ca. 2.0 Å), and Cu–Cu interatomic distance (ca. 4.7 Å). The correspondence between the simulated and experimental PDF data indicates that the structural parameters of **2a** are similar to those of **1**(BF_4),[19] even though the oxidation state is different. The peak assigned to the distance between nearest-neighbor copper centers (ca. 4.7 Å) suggests that the Cu atoms are bridged by the abpy ligands, consistent with the polymeric nature of **2a**. We also synthesized and crystallographically characterized $Cu(azpy)_2$ (azpy = phenylazo-2-pyridine; Figure 2B; Supporting Information, Table S1), a molecular analogue of $[Cu(abpy)]_n$. Molecular $Cu(azpy)_2$ crystallizes in the space group $Pna2_1$ with two crystallographically independent molecules in the unit cell in a distorted tetrahedral geometry with C–N bond distances from 1.35–1.41 Å and Cu–N distances of 1.9–2.0 Å (Supporting Information, Table S2). The PDF of $Cu(azpy)_2$, simulated from the crystal structure, is similar to that of **2a** but lacks the intense peak at about 4.7 Å, which supports the assignment of this peak as the Cu–Cu interatomic distance in **2a** (Supporting Information, Figure S7).

The infrared (IR) spectrum of **1a**(PF_6) exhibits peaks at 818 cm^{-1} and 554 cm^{-1}, corresponding to PF_6^- stretches (Supporting Information, Figure S8). These peaks are absent in the IR spectrum of **2a**, indicating the departure of PF_6^- anions to maintain charge balance upon chemical reduction. Additionally, a broad absorbance centered at about 2500 cm^{-1} appears in the IR spectrum of **2a**; this feature is absent in the IR spectrum of **1a**(PF_6) (Figure 2C). Analysis of the absorbance of **2a** in the UV/Vis-NIR region by diffuse-reflectance spectroscopy (Figure 2D) also reveals a low lying electronic excitation in the region of about 5000 cm^{-1} (limited by the instrumental detection range; Figure 2D) that is absent in the spectrum of **1a**(PF_6). Based on the observation of a similar band in the mixed-valence molecule $Cu(abpy)_2$ (which was transiently generated in an electrochemical cell),[20] this dominant low-energy band in **2a** is assigned as an intervalence charge transfer (IVCT) band. Maity et al. describe the mixed-valency in the molecular $Cu(abpy)_2$ as a Robin–Day[21] Class III system with $Cu^I(abpy^{0.5-})_2$, where one electron is delocalized over the two abpy ligands.[20] An IVCT band is a signature of mixed-valence,[22] and we therefore expect substantial electronic communication between the redox-active abpy ligands and the Cu centers in **2a**. The UV/Vis-NIR spectrum of **1a**(PF_6) has an intense band centered around 9100 cm^{-1} and a band around 26000 cm^{-1} (Figure 2D). Analogous bands had been observed for the cationic $[Cu(abpy)_2][PF_6]$ molecule and were assigned to a metal-to-ligand charge transfer (MLCT) transition and a π–π* transition, respectively.[20] These bands diminish upon reduction, consistent with electrons being added to the azo N=N π* orbital.[20]

The solid-state electron paramagnetic resonance (EPR) spectrum of **2a** is also indicative of considerable ligand radical character. The spectrum features a broad peak with a g value of 2.08 (Figure 3A; Supporting Information, Figure S9),

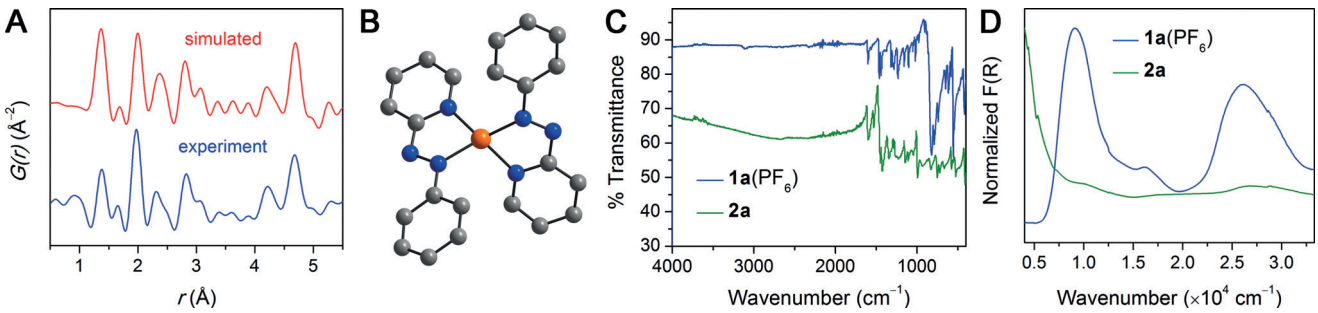

Figure 2. A) Simulated X-ray pair distribution function (PDF) of the previously reported **1**(BF_4)[10] without BF_4^- using Q_{max} = 23.7 $Å^{-1}$ (red) and the experimental PDF of **2a** (blue) with Q_{max} = 23.7 $Å^{-1}$. B) Single-crystal X-ray structure of $Cu(azpy)_2$ (azpy = phenylazo-2-pyridine), a molecular analogue of **2a**.[29] Cu orange, N blue, C gray. H atoms omitted for clarity. C) Mid-IR spectra of **1a**(PF_6) (blue) and **2a** (green). D) Normalized diffuse reflectance UV/Vis-NIR spectra of **1**(PF_6) (blue) and **2a** (green).

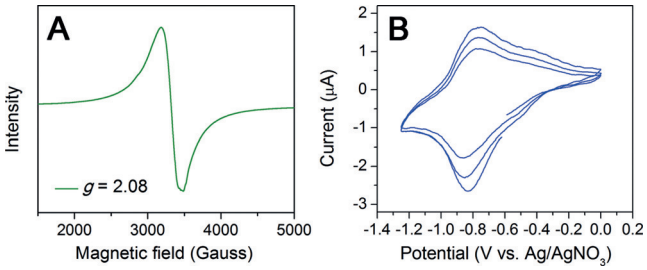

Figure 3. A) Solid-state EPR spectrum of **2a** measured at 77 K. B) Solid-state cyclic voltammograms of **2a** obtained at a scan rate of 2 $mV s^{-1}$. Scans started in the reductive direction.

consistent with a ligand-based radical with some delocalization over the metal. A ligand-based reduction would formally correspond to a polymer comprised of copper(I) centers, with azobispyridine radical mono-anions providing charge balance. Ligand-centered reduction of azopyridine ligands has precedent.[20,23,24] However, the g value of **2a** is slightly shifted from the free-electron g value ($g = 2.002$) expected for organic radicals, indicating that the unpaired electron resides in a molecular orbital with some Cu character.[20,25]

Electrochemical analysis of **1a**(PF_6)/**2a** was accomplished by electrodeposition of the polymer as a thin film on the surface of a glassy carbon (GC) working electrode from an electrolyte solution of 1 mM **1a**(PF_6) in 0.1M tetrabutylammonium hexafluorophosphate ($TBAPF_6$) in MeCN. Cyclic voltammograms (CVs) of the film reveal a broad redox event assigned to the oxidation and reduction of each repeat unit, with an $E_{1/2}$ of −0.82 V vs. $Ag/AgNO_3$ (Figure 3B). The broad peak width is most likely due to overlapping redox processes as each monomer unit of the chain is reduced.

The reported crystal structure of [Cu(abpy)BF_4]$_n$ **1**(BF_4) reveals that the BF_4^- counteranions occupy channels in between polymer chains.[19] The increase in porosity upon reduction of **1a**(PF_6) to **2a** (Figure 4A) suggests that the porosity arises from the loss of PF_6^- anions upon chemical reduction and that the resulting metallopolymer chains undergo limited structural relaxation. Voids created by inefficient packing of polymer chains in the solid state may also contribute to the observed porosity. Indeed, a pore-size-distribution analysis shows a variation ranging from micro- to mesopores (Supporting Information, Figure S10).

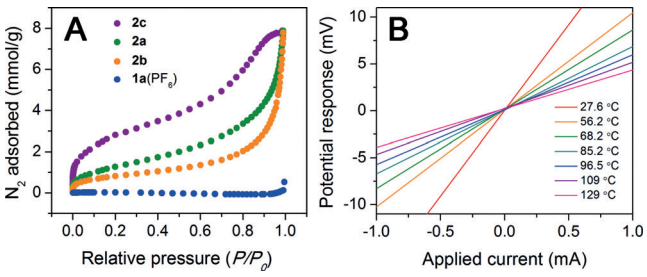

Figure 4. A) Nitrogen isotherms measured at 77 K of fine powders of **2c** (purple), **2a** (green), **2b** (orange), and **1a**(PF_6) (blue). B) Current–voltage curves of **2a**.

This hypothesis raised the intriguing possibility that the porosity of these reduced [Cu(abpy)]$_n$ coordination polymers might be tuned simply by choice of the appropriate counterion in the cationic [Cu(abpy)X]$_n$ precursor. To test that the porosity of the [Cu(abpy)]$_n$ polymers was associated with the loss of the counterion upon reduction of **1**(X), and to modulate the porosity of the [Cu(abpy)]$_n$ polymers, we chemically reduced two other compounds of the form [Cu(abpy)X]$_n$, $X^- = Br^-$(**1b**) and $X = BAr^{F-}$ (**1c**; BAr^{F-} = tetrakis(3,5-bis(trifluoromethyl)phenyl)borate), that contain counterions of different size. Analysis of the surface areas of the resulting powders (Table 1) reveal that the surface area of the [Cu(abpy)]$_n$ coordination polymers can be tuned by changing the identity and size of the anion X. Reduction of [Cu(abpy)PF_6]$_n$ **1a**(PF_6), [Cu(abpy)Br]$_n$ **1b**(Br), and [Cu(abpy)BAr^F]$_n$ **1c**(BAr^F) results in the [Cu(abpy)]$_n$ polymers **2a**, **2b**, and **2c** with BET surface areas of 90 $m^2 g^{-1}$, 60 $m^2 g^{-1}$, and 200 $m^2 g^{-1}$, respectively, with porosity increasing with the size of the counterion (Table 1, Figure 4A).

Polymers **2a** and **2b** are microporous and show a combination of Type I and II isotherms, according to the IUPAC classification.[26] We observe a filling of micropores in the low-pressure region, followed by continuous uptake at higher-pressures, corresponding to the filling of larger pores and possibly the voids between particles (Figures 4A).[27] In contrast, **2c** possesses a Type IV isotherm shape and hysteresis loop, indicating that the bulky BAr^{F-} anions induce mesoporosity in the material (Supporting Information, Figure S11).[26]

To probe the transport properties of these materials, we performed four-point-probe conductivity measurements on pellets pressed at two different pressures (Table 1) with electrodes placed in the van der Pauw configuration.[28] Upon reduction of **1a**(PF_6) to **2a**, the room-temperature conductivity increased by nine orders of magnitude (Supporting Information, Table S2). The conductivity of pellets of **2** (pressed at 22 kN) is 0.11 $S cm^{-1}$ at room temperature and increases to 0.45 $S cm^{-1}$ at 118 °C (Figure 4B). The temperature dependence of the conductivity indicates a thermally activated conduction process with an Arrhenius energy (E_a) of 150 meV (Supporting Information, Figure S18). Based on reports of other conductive coordination polymers and transport in class II mixed-valence systems, the mechanism of conduction is likely nearest-neighbor hopping.[13] Pellets of **2a**, **2b**, and **2c** pressed under two different conditions are all electrically conductive (Table 1) with conductivities in the range of 1.7×10^{-2} to 0.11 $S cm^{-1}$ (Table 1; Supporting Information, Figures S12–S22, Table S5). While the surface areas of the pressed pellets of **2** are lower than those of the powders isolated upon reduction of **1**(X) (Table 1), the trends in porosity (**2b** < **2a** < **2c**) are retained. Moreover, the magnitude of the conductivities of the pressed pellets do not show a strong correlation with the porosities of the pressed pellets (Table 1), implicating that the factors which contribute to the conductivity are decoupled from those which contribute to the porosity.

In conclusion, we show a new method for generating conductive porous coordination polymers by sculpting pores in polymers through templating effects by anions that leave

the framework upon reduction. When redox-active ligands are coupled to such polymers, this yields a general method for simultaneously increasing both conductivity and porosity in a single 1D coordination polymer. While the properties of coordination polymer chains have previously been shown to be sensitive to their redox state,[17] the ability to simultaneously convert a nonporous insulator to a porous conductor is unusual.

Acknowledgements

We thank the Office of Naval Research (ONR N000141410551, R.M.W) and the Center for Molecular Analysis and Design (CMAD, N.E.C, M.A.M.) for graduate fellowships. M.A.M. thanks CMAD, the National Science Foundation (NSF; award DGE-114747) and Stanford's Diversifying Academia, Recruiting Excellence Program for fellowships. D.U. thanks the Japanese Society for the Promotion of Science (JSPS) for a postdoctoral fellowship (JSPS Overseas Research Fellowship). Work by M.A.M., D.U., and H.I.K. was funded by an NSF CAREER award (DMR-1351538). We thank Prof. Christopher E. D. Chidsey and Dr. Michael Aubrey for helpful discussions, Dr. Lucy Darago, Matthew Smith, Adam Slavney, Katherine Walker, Elizabeth McLoughlin for experimental assistance, and Prof. Edward I. Solomon for access to equipment. Part of this work was performed at the Stanford Nano Shared Facilities (SNSF), supported by the NSF under award ECCS-1542152. We thank Kevin Beyer and Dr. Karena Chapman for performing the synchrotron measurements. This research used resources of the Advanced Photon Source, a U.S. Department of Energy (DOE) Office of Science User Facility operated for the DOE Office of Science by Argonne National Laboratory under Contract No. DE-AC02-06CH11357.

Conflict of interest

The authors declare no conflict of interest.

Keywords: microporous materials · N-ligands · polymers · redox chemistry · semiconductors

How to cite: *Angew. Chem. Int. Ed.* **2018**, *57*, 14585–14588
Angew. Chem. **2018**, *130*, 14793–14796

[1] S. R. Batten, N. R. Champness, X.-M. Chen, J. García-Martínez, S. Kitagawa, L. Öhrström, M. O'Keeffe, M. P. Suh, J. Reedijk, *Pure Appl. Chem.* **2013**, *85*, 1715–1724.
[2] G. R. Whittell, M. D. Hager, U. S. Schubert, I. Manners, *Nat. Mater.* **2011**, *10*, 176–188.
[3] B. J. Holliday, T. B. Stanford, T. M. Swager, *Chem. Mater.* **2006**, *18*, 5649–5651.
[4] B. J. Holliday, T. M. Swager, *Chem. Commun.* **2005**, 23–36.
[5] B. Le Ouay, M. Boudot, T. Kitao, T. Yanagida, S. Kitagawa, T. Uemura, *J. Am. Chem. Soc.* **2016**, *138*, 10088–10091.
[6] M. Ballesteros-Rivas, A. Ota, E. Reinheimer, A. Prosvirin, J. Valdés-Martinez, K. R. Dunbar, *Angew. Chem. Int. Ed.* **2011**, *50*, 9703–9707; *Angew. Chem.* **2011**, *123*, 9877–9881.
[7] Y. Zhang, S. N. Riduan, J. Wang, *Chem. Eur. J.* **2017**, *23*, 16419–16431.
[8] N. Casado, G. Hernández, H. Sardon, D. Mecerreyes, *Prog. Polym. Sci.* **2016**, *52*, 107–135.
[9] A. G. Slater, A. I. Cooper, *Science* **2015**, *348*, 988.
[10] O. Rivada-Wheelaghan, S. L. Aristizábal, J. López-Serrano, R. R. Fayzullin, J. R. Khusnutdinova, *Angew. Chem. Int. Ed.* **2017**, *56*, 16267–16271; *Angew. Chem.* **2017**, *129*, 16485–16489.
[11] M. Stollenz, J. E. Raymond, L. M. Pérez, J. Wiederkehr, N. Bhuvanesh, *Chem. Eur. J.* **2016**, *22*, 2396–2405.
[12] J.-X. Jiang, C. Wang, A. Laybourn, T. Hasell, R. Clowes, Y. Z. Khimyak, J. Xiao, S. J. Higgins, D. J. Adams, A. I. Cooper, *Angew. Chem. Int. Ed.* **2011**, *50*, 1072–1075; *Angew. Chem.* **2011**, *123*, 1104–1107.
[13] R. P. Kingsborough, T. M. Swager, *J. Am. Chem. Soc.* **1999**, *121*, 8825–8834.
[14] P.-L. Vidal, B. Divisia-Blohorn, G. Bidan, J.-L. Hazemann, J.-M. Kern, J.-P. Sauvage, *Chem. Eur. J.* **2000**, *6*, 1663–1673.
[15] W. R. Caseri, H. D. Chanzy, K. Feldman, M. Fontana, P. Smith, T. A. Tervoort, J. G. P. Goossens, E. W. Meijer, A. P. H. J. Schenning, I. P. Dolbnya, M. G. Debije, M. P. de Haas, J. M. Warman, A. M. van de Craats, R. H. Friend, H. Sirringhaus, N. Stutzmann, *Adv. Mater.* **2003**, *15*, 125–129.
[16] A. E. Rudenko, N. E. Clayman, J. K. Maclaren, R. M. Waymouth, *ChemistrySelect* **2016**, *1*, 3491–3496.
[17] I.-R. Jeon, L. Sun, B. Negru, R. P. Van Duyne, M. Dincă, T. D. Harris, *J. Am. Chem. Soc.* **2016**, *138*, 6583–6590.
[18] L. Sun, M. G. Campbell, M. Dincă, *Angew. Chem. Int. Ed.* **2016**, *55*, 3566–3579; *Angew. Chem.* **2016**, *128*, 3628–3642.
[19] C. S. Campos-Fernández, J. R. Galán-Mascarós, B. W. Smucker, K. R. Dunbar, *Eur. J. Inorg. Chem.* **2003**, 988–994.
[20] S. Maity, S. Kundu, T. Weyhermüller, P. Ghosh, *Inorg. Chem.* **2015**, *54*, 1300–1313.
[21] M. B. Robin, P. Day, *Adv. Inorg. Chem. Radiochem.* **1968**, *10*, 247–403.
[22] D. M. D'Alessandro, F. R. Keene, *Chem. Soc. Rev.* **2006**, *35*, 424–440.
[23] B. Sarkar, S. Patra, J. Fiedler, R. B. Sunoj, D. Janardanan, S. M. Mobin, M. Niemeyer, G. K. Lahiri, W. Kaim, *Angew. Chem. Int. Ed.* **2005**, *44*, 5655–5658; *Angew. Chem.* **2005**, *117*, 5800–5803.
[24] B. Sarkar, S. Patra, J. Fiedler, R. B. Sunoj, D. Janardanan, G. K. Lahiri, W. Kaim, *J. Am. Chem. Soc.* **2008**, *130*, 3532–3542.
[25] J. Takaichi, Y. Morimoto, K. Ohkubo, C. Shimokawa, T. Hojo, S. Mori, H. Asahara, H. Sugimoto, N. Fujieda, N. Nishiwaki, S. Fukuzumi, S. Itoh, *Inorg. Chem.* **2014**, *53*, 6159–6169.
[26] K. S. W. Sing, D. H. Everett, R. A. W. Haul, L. Moscou, R. A. Pierotti, J. Rouquérol, T. Siemieniewska, *Pure Appl. Chem.* **1985**, *57*, 603–619.
[27] M. Rose, N. Klein, W. Böhlmann, B. Böhringer, S. Fichtner, S. Kaskel, *Soft Matter* **2010**, *6*, 3918–3923.
[28] D. K. Schroder, *Semiconductor Material and Device Characterization*, 3rd ed., Wiley, Hoboken, **2006**.
[29] CCDC 1825140 contains the supplementary crystallographic data for this paper. These data are provided free of charge by The Cambridge Crystallographic Data Centre.

Manuscript received: June 29, 2018
Version of record online: September 19, 2018

